IOP Publishing | The Japan Society of Fluid Mechanics Fluid *Dynamics* Research

Fluid Dyn. Res. **47** (2015) 015504 (11pp) doi:10.1088/0169-5983/47/1/015504

Exact coherent structures in an asymptotically reduced description of parallel shear flows

Cédric Beaume[1,4], Edgar Knobloch[1], Gregory P Chini[2] and Keith Julien[3]

[1] Department of Physics, University of California, Berkeley, CA 94720, USA
[2] Department of Mechanical Engineering & Program in Integrated Applied Mathematics, University of New Hampshire, Durham NH, 03824, USA
[3] Department of Applied Mathematics, University of Colorado at Boulder, Boulder, CO 80309, USA

E-mail: ced.beaume@gmail.com, knobloch@berkeley.edu, greg.chini@unh.edu and keith.julien@colorado.edu

Received 27 May 2014, revised 9 September 2014
Accepted for publication 3 October 2014
Published 29 October 2014

Communicated by M Funakoshi

Abstract

A reduced description of shear flows motivated by the Reynolds number scaling of lower-branch exact coherent states in plane Couette flow (Wang J, Gibson J and Waleffe F 2007 *Phys. Rev. Lett.* **98** 204501) is constructed. Exact time-independent nonlinear solutions of the reduced equations corresponding to both lower and upper branch states are found for a sinusoidal, body-forced shear flow. The lower branch solution is characterized by fluctuations that vary slowly along the critical layer while the upper branch solutions display a bimodal structure and are more strongly focused on the critical layer. The reduced equations provide a rational framework for investigations of sub-critical spatiotemporal patterns in parallel shear flows.

(Some figures may appear in colour only in the online journal)

1. Introduction

Exact nonlinear solutions of the equations describing the evolution of simple parallel shear flows have proved to be of immense value (Kawahara *et al* 2012). The existence of these

[4] Current affiliation: Department of Aeronautics, Imperial College London, London SW7 2AZ, UK.

solutions exposes the basic mechanism underlying self-sustained structures in shear flows and may ultimately shed light on the properties of subcritical turbulence in these flows. However, despite notable success (Nagata 1990, Clever and Busse 1997, Waleffe 1997, Gibson *et al* 2008, Schneider *et al* 2010, Brand and Gibson 2014, Gibson and Brand 2014, Khapko *et al* 2014, Lucas and Kerswell 2014a) the computation of such 'exact coherent states/ structures' (ECS) remains difficult because they are three-dimensional (3D) and disconnected from the structureless base shear flow. In addition, much insight into the complex dynamics exhibited by transitional flows has come from viewing the flow in terms of a temporal sequence of transitions between weakly unstable coherent structures (Auerbach *et al* 1987, Christiansen *et al* 1997, Halcrow *et al* 2009). This notion has met with great success, but depends on our ability to identify a large number of ECS in these flows and the connections between them (Duguet *et al* 2008, Chandler and Kerswell 2013, Lucas and Kerswell 2014b). In this paper we propose a systematic but general procedure that leads to a simplified but self-consistent description of the required ECS. Our approach differs in certain important aspects from the pioneering analysis of Hall and Sherwin (2010) and builds on earlier work by the authors (Chini *et al* 2009, Beaume 2012). Specifically, we derive a simplified version of the governing partial differential equations (PDEs) that yields an asymptotically exact description of lower branch states in the limit $Re \to \infty$, where Re is a suitably defined Reynolds number. We propose a *composite* multiscale PDE model that is uniformly valid over the entire spatial domain. Our model has much in common with the hybrid formulation of Blackburn *et al* (2013), but was developed independently (Beaume 2012). Moreover, our derivation highlights the underlying PDE structure associated with the formation of ECS and, although not pursued here, also reveals how slow streamwise modulation of the mean (streamwise-invariant) and fluctuation (streamwise-varying) fields may be consistently incorporated. We solve the resulting equations by an iterative scheme, each step of which requires the solution of a two-dimensional problem only. We demonstrate the method on a sinusoidal, body-forced shear flow with stress-free boundaries that we call Waleffe flow, a flow first introduced by Drazin and Reid (1981) and further studied by Waleffe (1997). Remarkably, for this flow our method not only captures the lower branch states for which it was developed, but also *upper branch* states: in spite of the large Re formulation, the asymptotics prove sufficiently robust to capture the saddle-node bifurcation giving rise to these solutions. For the domain size used, this bifurcation occurs at $Re \approx 136$ and we are able to numerically continue both branches from this value to $Re > 2000$. The continuation allows us to study the evolution of the detailed structure of Waleffe flow ECS with increasing Re; this structure differs from that of Couette flow ECS.

2. Asymptotic reduction

We consider incompressible flow driven by a streamwise body force that varies sinusoidally in the wall-normal (y) direction (Drazin and Reid 1981, Waleffe 1997, Beaume 2012)

$$\partial_t \mathbf{u} + (\mathbf{u} \cdot \nabla)\mathbf{u} = -\nabla p + \frac{1}{Re}\nabla^2 \mathbf{u} + \frac{\sqrt{2}\,\pi^2}{4\,Re} \sin\left(\frac{1}{2}\pi y\right)\hat{\mathbf{x}}, \tag{1}$$

$$\nabla \cdot \mathbf{u} = 0, \tag{2}$$

subject to stress-free boundary conditions at stationary walls located at $y = \pm 1$

$$\partial_y u = v = \partial_y w = 0. \tag{3}$$

Here $Re \equiv UH/\nu$ is the Reynolds number, where H is the channel half-width and U is the root-mean-square velocity of the base flow given in dimensionless form by $(u, v, w) = (\sqrt{2}\sin(\pi y/2), 0, 0)$, hereafter referred to as Waleffe flow. Like the more extensively studied plane Couette flow (PCF), Waleffe flow is linearly stable for all Re but may be unstable to finite amplitude perturbations. The codimension-one states on the boundary separating the basin of attraction of Waleffe flow from that of the upper branch states are called edge states (Skufca *et al* 2006) and are typically found on lower branches. These nonlinear states are maintained against decay by the self-sustaining instability mechanism elucidated by Waleffe (1997) and further clarified at large Reynolds number by Hall and Sherwin (2010).

Given the occurrence of streamwise streaks and rolls that typify ECS in shear flows, we decompose the velocity vector into a streamwise component and a perpendicular vector, i.e., $\mathbf{v} = (u, \mathbf{v}_\perp)$, where $\mathbf{v}_\perp = (v, w)$, and posit appropriate asymptotic expansions for the various fields. To this end, we are motivated in part by the scaling behavior identified by Wang *et al* (2007) for lower-branch ECS in PCF. As indicated by this scaling the rolls comprising the streamwise-invariant flow in the perpendicular plane are weak, of $O(\epsilon)$ amplitude, where $\epsilon \equiv 1/Re$, relative to the deviation of the streamwise-invariant streamwise flow from the base laminar profile (i.e., relative to the streaks). A *closed* and asymptotically consistent reduced description may be obtained by further positing that the (streamwise-varying) fluctuations are similarly weak relative to the mean streamwise flow, an assumption consistent with the scaling behavior reported by Wang *et al* (2007). We suppose that all fields are functions of (x, X, y, z, t, T), where $X \equiv \epsilon x$ and $T \equiv \epsilon t$ are slow scales (Chini *et al* 2009), and write

$$u \sim \bar{u}_0 + \epsilon\left(\bar{u}_1 + u_1'\right) + \ldots, \tag{4}$$

$$\mathbf{v}_\perp \sim \epsilon\left(\bar{\mathbf{v}}_{1\perp} + \mathbf{v}_{1\perp}'\right) + \ldots, \tag{5}$$

$$p \sim \bar{p}_0 + \epsilon\left(\bar{p}_1 + p_1'\right) + \epsilon^2\left(\bar{p}_2 + p_2'\right) + \ldots, \tag{6}$$

where an overbar denotes a 'fast' (x, t) average and a prime denotes a fluctuation with zero fast mean. Substituting these expansions into the multiscale versions of equations (1), (2), collecting terms at like order in ϵ, and parsing the resulting equations into mean and fluctuating components yields the following asymptotically-reduced, multiscale PDE system:

$$\partial_T\bar{u}_0 + \bar{u}_0\partial_X\bar{u}_0 + \left(\bar{\mathbf{v}}_{1\perp}\cdot\nabla_\perp\right)\bar{u}_0 = -\partial_X\bar{p}_0 + \frac{\sqrt{2}\pi^2}{4}\sin\left(\frac{\pi y}{2}\right) + \nabla_\perp^2\bar{u}_0, \tag{7}$$

$$\partial_T\bar{\mathbf{v}}_{1\perp} + \partial_X[\bar{u}_0\bar{\mathbf{v}}_{1\perp}] + \nabla_\perp\cdot\left[\bar{\mathbf{v}}_{1\perp}\bar{\mathbf{v}}_{1\perp} + \overline{\mathbf{v}_{1\perp}'\mathbf{v}_{1\perp}'}\right] = -\nabla_\perp\bar{p}_2 + \nabla_\perp^2\bar{\mathbf{v}}_{1\perp}, \tag{8}$$

$$\partial_X\bar{u}_0 + \nabla_\perp\cdot\bar{\mathbf{v}}_{1\perp} = 0, \tag{9}$$

which govern the mean dynamics, and

$$\partial_t u_1' + \bar{u}_0\partial_x u_1' + \left(\bar{\mathbf{v}}_{1\perp}'\cdot\nabla_\perp\right)\bar{u}_0 = -\partial_x p_1' + \epsilon\nabla_\perp^2 u_1', \tag{10}$$

$$\partial_t\mathbf{v}_{1\perp}' + \bar{u}_0\partial_x\mathbf{v}_{1\perp}' = -\nabla_\perp p_1' + \epsilon\nabla_\perp^2\mathbf{v}_{1\perp}', \tag{11}$$

$$\partial_x u_1' + \nabla_\perp\cdot\mathbf{v}_{1\perp}' = 0, \tag{12}$$

which govern the fluctuating fields. Here, $\nabla_\perp$ is the gradient operator in the (y, z) plane. Note that $\bar{p}_0 = \bar{p}_0(X, T)$ is set to zero for Waleffe flow and PCF, but may be retained for flows driven by externally-imposed pressure gradients, such as plane Poiseuille flow. We emphasize that equations (7)–(12) comprise a *closed* reduced system; the usual closure issues resulting

from averaging do not arise here owing to our ability to exploit scale separation. Physically, the averaged equations constrain the slow temporal and streamwise evolution of the streaks ($\bar{u}_0$) and rolls ($\bar{\mathbf{v}}_{1\perp}$). The presence of an effective Reynolds number equal to unity and the elimination of fast streamwise and temporal variation in these equations facilitate both time-stepping and the computation of equilibrium ECS in comparison with equations (1), (2) at $Re \gg 1$. Further savings accrue if the slow streamwise (X) variation is suppressed, as in our computations here, since the averaged equations are then spatially 2D.

Presuming fluctuation gradients remain $O(1)$, the fluctuating fields themselves evolve in accord with the equations governing the *inviscid secondary stability* of streamwise streaks. The fluctuation fields, which are necessarily steady (i.e., neutrally stable) for equilibrium ECS, exhibit a critical layer structure along the isosurface $\bar{u}_0(y, z) = 0$ (Maslowe 1986, Hall and Sherwin 2010). In the neighborhood of the critical layer, fluctuation gradients are large, resulting in a distinct leading-order dominant balance of terms involving diffusion. However, we choose to avoid the intricacies associated with carrying out a systematic matched asymptotic analysis to address the critical layer singularity. Instead we retain the formally small perpendicular diffusion terms in equations (10), (11), which are then uniformly valid over the entire spatial domain. Retention of these terms may be justified by appeal to the method of *composite asymptotic equations*, as in Giannetti and Luchini (2006).

It is important to note that the fluctuation equations are quasilinear and therefore do not mix x modes, a fact that we exploit in our computations of ECS for Waleffe flow using the reduced system. In fact, in accord with the scalings found by Wang *et al* (2007), we retain only a *single* streamwise Fourier mode for each fluctuation field: $[u_1', \mathbf{v}_{1\perp}', p_1'](x, y, z, t) = [u_1, \mathbf{v}_{1\perp}, p_1](y, z, t)\mathrm{e}^{\mathrm{i}\alpha x}$ + c.c., where c.c. denotes complex conjugate and $\alpha = 2\pi/L_x$ is the fundamental dimensionless streamwise wavenumber. Before describing the computation of *streamwise uniform* ECS, we remark that in long domains a nearly continuous band of modes with similar streamwise wavenumbers will be neutral or very weakly damped. Hence, a linear superposition of these fluctuation modes will naturally induce a *slowly-varying* envelope, $A(X, T)$ say, that will in turn drive slow streamwise modulations of the mean fields through the Reynolds stress divergence term in equation (8). If realized, this multiscale coupling may provide a mechanism for streamwise localization of ECS in a variety of plane parallel shear flows, further attesting to the value of the reduced PDE structure identified here.

With X derivatives suppressed, equations (7)–(9) can be further simplified by introducing a streamwise-invariant streamfunction $\phi_1(y, z)$ so that $\bar{v}_1 = -\partial_z\phi_1$ and $\bar{w}_1 = \partial_y\phi_1$, and the corresponding streamwise vorticity $\omega_1 = \nabla_\perp^2\phi_1$, resulting in the following set of equations:

$$\partial_T u_0 + J\left(\phi_1, u_0\right) = \nabla_\perp^2 u_0 + \frac{\sqrt{2}\pi^2}{4}\sin\left(\frac{1}{2}\pi y\right), \tag{13}$$

$$\partial_T\omega_1 + J\left(\phi_1, \omega_1\right) + 2\left(\partial_{yy}^2 - \partial_{zz}^2\right)\left(\mathcal{R}\left(v_1 w_1^*\right)\right) + 2\partial_y\partial_z\left(w_1 w_1^* - v_1 v_1^*\right) = \nabla_\perp^2\omega_1, \tag{14}$$

where $J(\phi_1, f) \equiv \partial_y\phi_1\partial_z f - \partial_z\phi_1\partial_y f$, f^* denotes the complex conjugate of f, and $\mathcal{R}(f)$ denotes its real part; since $u_0' \equiv 0$ the overbar on the $O(1)$ streaky flow component has been omitted. The fluctuation equations can be written in the more useful form

$$\left(\alpha^2 - \nabla_\perp^2\right)p_1 = 2\mathrm{i}\alpha\left(v_1\partial_y u_0 + w_1\partial_z u_0\right), \tag{15}$$

$$\partial_t\mathbf{v}_{1\perp} + \mathrm{i}\alpha u_0\mathbf{v}_{1\perp} = -\nabla_\perp p_1 + \epsilon\nabla_\perp^2\mathbf{v}_{1\perp}. \tag{16}$$

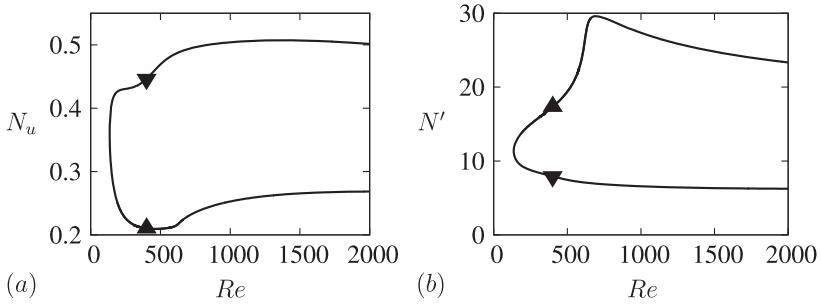

Figure 1. Bifurcation diagram showing the lower (downward triangle) and upper (upward triangle) branches of ECS as a function of the Reynolds number Re in terms of (a) $N_u = \int_D u_0^2 \, \mathrm{d}y \, \mathrm{d}z / \int_D \mathrm{d}y \, \mathrm{d}z$, (b) $N' = \int_D (v_1^2 + w_1^2) \, \mathrm{d}y \, \mathrm{d}z / \int_D \mathrm{d}y \, \mathrm{d}z$. The branches are connected via a saddle-node bifurcation at $Re \approx 136$. Lower branch states are computed on a 32×64 mesh while upper branch states are computed on a 64×128 mesh.

Note that u_1 is not required to close the equations although it may also be computed. In the following these equations are solved subject to stress-free and no normal-flow boundary conditions

$$\partial_y u_0 = \omega_1 = \phi_1 = v_1 = \partial_y w_1 = 0, \quad \text{at} \quad y = \pm 1. \tag{17}$$

Equations (15), (16) are homogeneous and quasilinear with solutions that depend on the slowly evolving streamwise velocity u_0. The solutions of these equations therefore either grow or decay. Since we are interested in stationary solutions of equations (1), (2) we use an iterative scheme consisting of two steps: searching for neutrally stable solutions of equations (15), (16) on the fast time scale t, and converging u_0 to a stationary state on the slow time scale T. We solve this problem on a two-dimensional domain $\mathcal{D}$ of size $L_y \times L_z = 2 \times \pi$, where L_y is the dimensionless gap and L_z is an imposed dimensionless period in the spanwise direction, and set $\alpha = 0.5$. In PCF this choice of domain leads to edge states with a single unstable direction (Schneider *et al* 2008). The computations are performed in spectral space using a mixed Fourier cosine/sine basis. Once a steady nontrivial solution has been found numerical continuation in Re is applied to trace out the whole solution branch. For simplicity we impose the shift-reflect symmetry $[u, v, w](x, y, z) = [u, v, -w](x + L_x/2, y, -z)$ observed in the corresponding solutions in PCF (Schneider *et al* 2008), where $L_x = 4\pi$ is the imposed period of the solution in the streamwise direction. All solutions reported here are numerically converged, as confirmed by doubling the spatial resolution and verifying that important quantities like energies and spectra change negligibly. The details of the iterative scheme used to solve this problem are nontrivial and will be described elsewhere (Beaume *et al* 2014) together with details of the continuation scheme.

3. Exact coherent states

Figure 1 shows the results in terms of $N_u \equiv \int_D u_0^2 \, \mathrm{d}y \, \mathrm{d}z \big/ \int_D \mathrm{d}y \, \mathrm{d}z$, measuring the strength of the streaks, and $N' \equiv \int_D (v_1^2 + w_1^2) \, \mathrm{d}y \, \mathrm{d}z \big/ \int_D \mathrm{d}y \, \mathrm{d}z$, measuring the strength of the associated spanwise fluctuations (v_1, w_1). These quantities are related to the kinetic energies per unit volume associated with these modes by $E_u = N_u/2$ and $E' = N'/(2\,Re^2)$. The figure shows that the reduced system captures not only the lower branch states for which it was

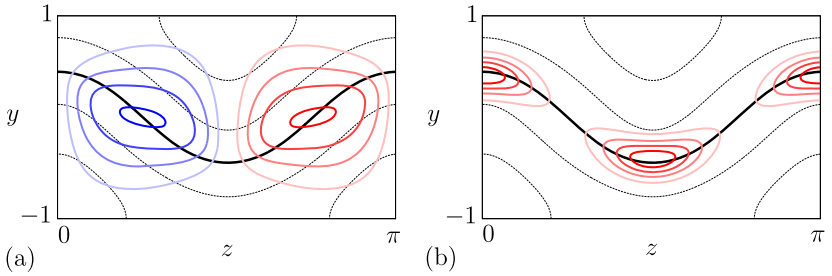

Figure 2. The lower branch solution at $Re \approx 1500$ represented by (a) contours of the streamwise-invariant streamfunction ϕ_1 and (b) the quantity $\| (v_1, w_1) \|_{L_2}$, a measure of spanwise fluctuations. In each plot positive (negative) values are indicated in red (blue). The contour plots are superposed on the streak profile shown in black, with the thick solid line representing the critical layer $u_0 = 0$. All contours are equidistributed.

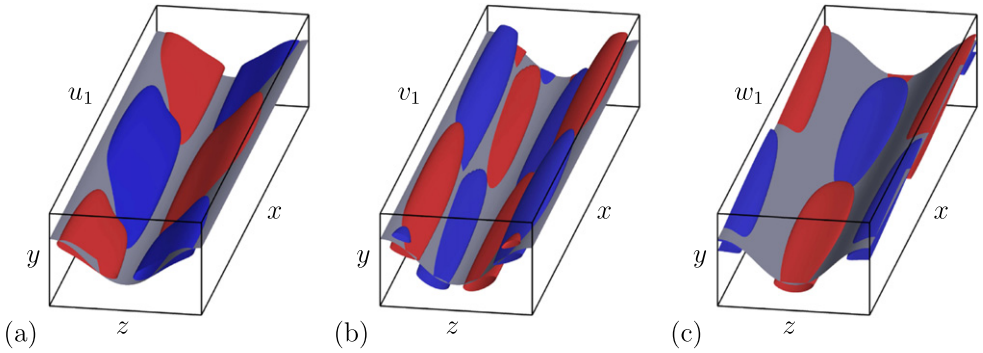

Figure 3. 3D rendition of the fluctuating flow on the lower branch solution at $Re \approx 1500$. The surfaces represented in color correspond to (a) $\frac{1}{2}\max|u_1|$, (b) $\frac{1}{2}\max|v_1|$, and (c) $\frac{1}{2}\max|w_1|$, with red (blue) representing positive (negative) values. The surface shown in grey represents the critical layer $u_0 = 0$.

developed but the upper branch states as well. The two branches connect via a saddle-node bifurcation at $Re \approx 136$.

Figure 2 shows streamwise-invariant representations of the lower branch solution at $Re \approx 1500$ while figure 3 provides insight into the 3D structure of this solution. Figures 4 and 5 provide analogous representations of the upper branch solution at the same Reynolds number. The lower branch solution is characterized by a smoothly undulating critical layer that is maintained by two nearly circular rolls (figure 2(a)). This structure is supported by fluctuations that concentrate along a critical layer of $O(\alpha\, Re\,)^{-1/3}$ width (Maslowe 1986, Wang *et al* 2007, Hall and Sherwin 2010). Figure 2(b) reveals that these fluctuations vary rapidly in the direction perpendicular to the critical layer with a much slower variation along it. The 3D representation in figure 3 confirms these observations and sheds more light on the streamwise dynamics of the lower branch solution: the streamwise velocity fluctuation u_1 is concentrated in the regions of strong streamwise-invariant streamfunction ϕ_1 (compare figure 2(a) with 3(a)) and therefore away from the extrema of the critical layer. In contrast, spanwise fluctuations (v_1, w_1) accumulate at the extrema of the critical layer (figure 2(b)), a

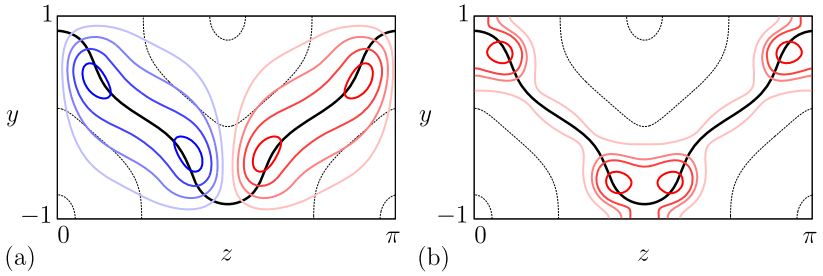

Figure 4. Same as figure 2 but for the upper branch solution at $Re \approx 1500$.

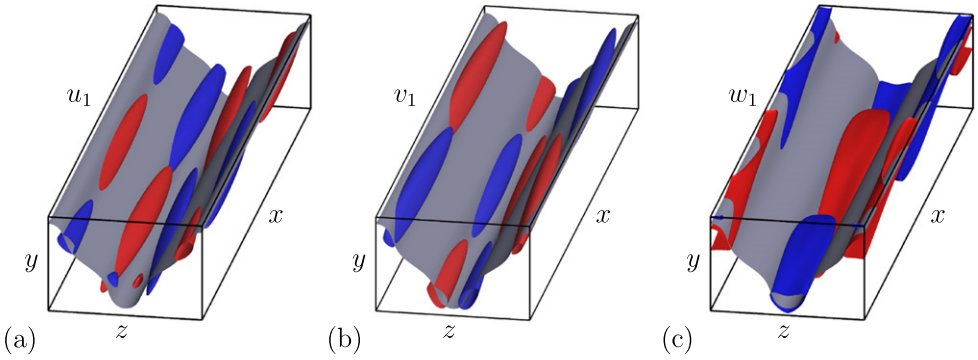

Figure 5. Same as figure 3 but for the upper branch solution at $Re \approx 1500$. Intersections of the fluctuation contours with the walls at $y = \pm 1$ that can be observed in (c) are a consequence of the stress-free boundary conditions.

consequence of the incompressibility of the fluctuations (equation (12)). At $x = 0$ (defined arbitrarily as the front section in figure 3), the fluid in the region around the lowest (respectively, highest) point of the critical layer tracks the critical layer from left to right (respectively, right to left); the directions are reversed at locations displaced half a period in the streamwise direction. Figure 6 shows projections of the fluctuations onto the critical layer $u_0 = 0$, where they are concentrated. The fluctuations do not consist of straight, x-oriented, vortices. Rather, their structure is oblique, stretched by the differential forcing in y, and the fluctuation intensity peaks close to $z = 0$ and $z = \pi/2$, where the critical layer departs strongly from the center of the domain $y = 0$.

In contrast with the nearly sinusoidal critical-layer profile exhibited by the lower branch solution, the critical layer associated with the upper branch solution is much more strongly deformed from the plane $y = 0$, even approaching at its extrema the top and bottom walls. This change of shape is a signature both of less coherent roll motion and of the splitting of each roll into a bimodal structure (figure 4(a)). This splitting moves the maxima of the streamwise-invariant streamfunction closer to the extrema of the critical layer to support its highly distorted profile. Figures 5(a)–(c) show that the fluctuations associated with this state exhibit properties similar to those on the lower branch: the spanwise fluctuations (v_1, w_1) are concentrated at the extrema of the critical layer with the streamwise velocity fluctuation u_1 expelled from these regions. However, the fluctuations also exhibit a bimodal structure with maximum values now located on either side of the critical layer extrema (figure 4(b)). This splitting serves to confine the critical layer in these regions, and leads to strong gradients in

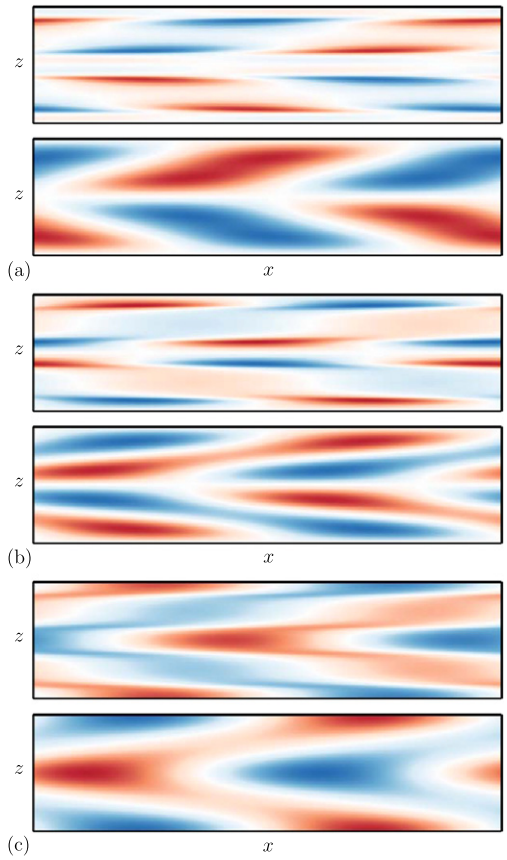

Figure 6. The fluctuations (a) u_1, (b) v_1 and (c) w_1 along the critical surface $u_0 = 0$. In each of these plots, the top panel represents the upper branch solution and the lower panel the lower branch solution. Red (blue) denotes positive (negative) values with the scale reset between plots and between the lower and upper branch solutions.

the fluctuation kinetic energy *along* the critical layer. Differences between the lower and upper branch states are reflected in the Fourier spectra of the associated fluctuation fields (figure 7). The figure shows the normalized partial sums

$$\Sigma_y(m_y) = \frac{1}{2(M-1)N}\left(S^2\left(m_y, 0\right) + \sum_{m_z=1}^{N} S^2(m_y, m_z) + S^2(m_y, -m_z)\right)^{1/2}, \tag{18}$$

$$\Sigma_z(m_z) = \frac{1}{2(M-1)N}\left(\sum_{m_y=0}^{M} S^2(m_y, m_z)\right)^{1/2}, \tag{19}$$

where $S^2(m_y, m_z) \equiv |v_1(m_y, m_z)|^2 + |w_1(m_y, m_z)|^2$ and M (respectively N) is the maximum wavenumber in the y (respectively z) direction. The quantity $\Sigma_y(m_y)$ (respectively $\Sigma_z(m_z)$) is therefore related to the energy in modes with wavenumber m_y (respectively m_z) in the y (respectively z) direction. The plots indicate that the magnitude of the fluctuations associated with upper branch solutions is larger than that for lower branch solutions. The fact that

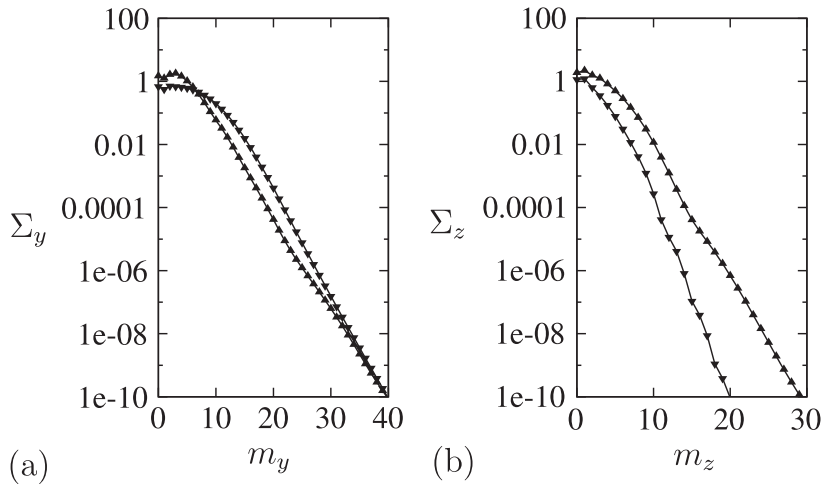

Figure 7. Spectral decomposition of the lower (downward triangles, figures 2 and 3) and upper (upward triangles, figures 4 and 5) branch solutions at $Re = 1500$ in terms of the normalized partial sums $\sum_y(m_y)$ in (a) and $\sum_z(m_z)$ in (b) defined in the text.

solutions along both branches exhibit similar decay in m_y (figure 7(a)) indicates that the wall-normal structure of the critical layer is similar along both branches. However, the slower decay in m_z along the upper branch indicates the presence of steeper variations in z along the upper branch, i.e., of solutions that are more strongly localized along the critical layer. These conclusions are confirmed in (x, z) plots of the fluctuations along the critical layer in figure 6. The dependence of the upper-branch fluctuations transverse to the critical layer is more abrupt than for the lower branch solution, with strong additional variation along the critical layer near the critical layer extrema at $z = 0$ and $z = \pi/2$. Indeed, the upper-branch fluctuations focus close to the extrema, but plateau away from these points. Comparison of the solutions found here and Nagata's solution for PCF (figure 7 of Jimenez *et al* 2005) reveals substantial similarity: the overall shape of the critical layer, location of the fluctuations and differences between the lower and upper branch states are all quite similar to those in PCF. These common features suggest that our solutions may play a similar role in Waleffe flow to that played by the Nagata solutions in PCF: separating relaminarizing perturbations from turbulence-generating perturbations (lower branch ECS) and capturing the statistical properties of the turbulent state (upper branch ECS). However, our solutions differ from the corresponding PCF solutions in the level of distortion of the critical layer along the upper branch, a difference we attribute to the different nature of the flow and in particular to the more benign stress-free boundary conditions used in the present work.

4. Summary and conclusion

We have described an asymptotic reduction procedure suggested by the lower branch scaling for PCF that appears to apply to parallel shear flows in general. The multiscale asymptotic approach adopted here results in a straightforward derivation of a reduced system of PDEs detailing the interaction between small scale fluctuations and streamwise-invariant structures that serves as a starting point for more detailed investigations. We have used this system to compute both lower and upper branch ECS for Waleffe flow using the Reynolds number *Re*

as a homotopy parameter that enabled us to continue the lower branch states into upper branch states. While we do not expect our solutions to be quantitatively accurate for $Re = O(1)$, i.e., near the saddle-node, the upper branch states obtained by continuation to large Re are expected to provide an accurate approximation to the upper branch ECS of the full 3D problem, just like the corresponding lower branch states. For these computations the use of Waleffe flow is advantageous since the application of stress-free boundary conditions enables us to employ and refine a *uniform* computational grid associated with a trigonometric basis in all coordinate directions.

Our lower branch solutions are qualitatively similar to those for PCF, but the upper branch solutions reveal properties heretofore unknown. These center on the appearance of a bimodal structure in both the streamwise rolls and the associated fluctuations. In an independent study, a similar asymptotic approach has recently been used to obtain lower branch solutions to PCF (Hall and Sherwin 2010, Blackburn *et al* 2013) but no upper branch states were reported.

In future work we will report on the stability properties of these states, including slow streamwise variation, and on their relation to the ECS of the full 3D problem. In addition, new ECS can be identified in the vicinity of the saddle-node captured by the reduced equations and continued to large Re, where they can be used to find the corresponding states of the full 3D problem. We mention finally that although these equations were derived for a parallel shear flow, the inclusion of slow streamwise variability suggests a systematic path for computing ECS in *developing* flows, including boundary layers.

Acknowledgments

This work was initiated during the 2008 NCAR Geophysical Turbulence Phenomena workshop in Boulder, CO, and developed during the Geophysical Fluid Dynamics Program at the Woods Hole Oceanographic Institution in 2012 (Beaume 2012). The authors gratefully acknowledge support from the National Science Foundation under grants No. DMS-1211953 and 1317596 (CB & EK), No. OCE-0934827 (GPC), and No. OCE-0934737 and DMS-1317666 (KJ). EK also acknowledges support from a Chaire d'Excellence Pierre de Fermat of the Région Midi-Pyrénées, France.

References

Auerbach D, Cvitanović P, Eckmann J-P, Gunaratne G and Procaccia I 1987 Exploring chaotic motion through periodic rrbits *Phys. Rev. Lett.* **58** 2387–9

Beaume C 2012 A reduced model for exact coherent states in high Reynolds numbers shear flows *Proc. Geophysical Fluid Dynamics Program (Woods Hole Oceanographic Institution)* pp 389–412

Beaume C, Chini G P, Julien K and Knobloch E 2014 Reduced description of exact coherent states in parallel shear flows (arXiv:1407.2980)

Brand E and Gibson J F 2014 A doubly localized equilibrium solution of plane Couette flow *J. Fluid Mech.* **750** R3

Blackburn H M, Hall P and Sherwin S J 2013 Lower branch equilibria in Couette flow: the emergence of canonical states for arbitrary shear flows *J. Fluid Mech.* **726** R2

Chandler G J and Kerswell R R 2013 Invariant recurrent solutions embedded in a turbulent two-dimensional Kolmogorov flow *J. Fluid Mech.* **722** 554–95

Chini G P, Julien K and Knobloch E 2009 An asymptotically reduced model of turbulent Langmuir circulation *Geophys. Astrophys. Fluid Dyn.* **103** 179–97

Christiansen F, Cvitanović P and Putkaradze V 1997 Spatiotemporal chaos in terms of unstable recurrent patterns *Nonlinearity* **10** 55–70

Clever R M and Busse F H 1997 Tertiary and quaternary solutions for plane Couette flow *J. Fluid Mech.* **344** 137–53
Drazin P and Reid W 1981 *Hydrodynamic Stability* (Cambridge: Cambridge University)
Duguet Y, Willis A P and Kerswell R R 2008 Transition in pipe flow: the saddle structure on the boundary of turbulence *J. Fluid Mech.* **613** 255–74
Giannetti F and Luchini P 2006 Leading-edge receptivity by adjoint methods *J. Fluid Mech.* **547** 21–53
Gibson J F, Halcrow J and Cvitanović P 2008 Visualizing the geometry of state space in plane Couette flow *J. Fluid Mech.* **611** 107–30
Gibson J F and Brand E 2014 Spanwise-localized solutions of planar shear flows *J Fluid Mech.* **745** 25–61
Halcrow J, Gibson J F, Cvitanović P and Viswanath D 2009 Heteroclinic connections in plane Couette flow *J. Fluid Mech.* **621** 365–76
Hall P and Sherwin S 2010 Streamwise vortices in shear flows: harbingers of transition and the skeleton of coherent structures *J. Fluid Mech.* **661** 178–205
Jimenez J, Kawahara G, Simens M P, Nagata M and Shiba M 2005 Characterization of near-wall turbulence in terms of equilibrium and 'bursting' solutions *Phys. Fluids* **17** 015105
Kawahara G, Uhlmann M and van Veen L 2012 The significance of simple invariant solutions in turbulent flows *Annu. Rev. Fluid Mech.* **44** 203–25
Khapko T, Duguet Y, Kreilos T, Schlatter P, Eckhardt B and Henningson D S 2014 Complexity of localised coherent structures in a boundary layer flow *Eur. Phys. J.* E **112** 32–45
Lucas D and Kerswell R R 2014a Spatiotemporal dynamics in 2D Kolmogorov flow over large domains *J. Fluid Mech.* **750** 518–54
Lucas D and Kerswell R R 2014b Recurrent flow analysis in spatiotemporally chaotic 2D Kolmogorov flow (arXiv:1406.1820)
Maslowe S A 1986 Critical layers in shear flows *Annu. Rev. Fluid Mech.* **18** 405–32
Nagata M 1990 Three-dimensional finite-amplitude solutions in plane Couette flow: bifurcation from infinity *J. Fluid Mech.* **217** 519–27
Schneider T M, Gibson J F, Lagha M, de Lillo F and Eckhardt B 2008 Laminar-turbulent boundary in plane Couette flow *Phys. Rev.* E **78** 037301
Schneider T M, Gibson J F and Burke J 2010 Snakes and ladders: localized solutions of plane Couette flow *Phys. Rev. Lett.* **104** 104501
Skufca J D, Yorke J A and Eckhardt B 2006 Edge of chaos in parallel shear flow *Phys. Rev. Lett.* **96** 174101
Waleffe F 1997 On a self-sustaining process in shear flows *Phys. Fluids* **9** 883–900
Wang J, Gibson J and Waleffe F 2007 Lower branch coherent states in shear flows: transition and control *Phys. Rev. Lett.* **98** 204501